Nuclear Engineering and Technology 55 (2023) 2356–2365

Contents lists available at ScienceDirect

Nuclear Engineering and Technology

journal homepage: www.elsevier.com/locate/net

Original Article

Applicability of abrasive waterjet cutting to irradiated graphite decommissioning

Francesco Perotti [a, b], Eros Mossini [c, *], Elena Macerata [c], Massimiliano Annoni [a], Michele Monno [a]

[a] Politecnico di Milano, Dipartimento di Meccanica, Via Giuseppe La Masa 1, 20156, Milano, Italy
[b] Consorzio MUSP, Strada Torre della Razza, 29122, Piacenza, Italy
[c] Politecnico di Milano, Dipartimento di Energia, P.za L. da Vinci 32, 20133, Milano, Italy

ARTICLE INFO

Article history:
Received 9 December 2022
Received in revised form
24 February 2023
Accepted 20 March 2023
Available online 23 March 2023

Keywords:
Abrasive waterjet cutting
Nuclear decommissioning
Jet power
Irradiated graphite

ABSTRACT

Characterization, dismantling and pre-disposal management of irradiated graphite (i-graphite) have an important role in safe decommissioning of several nuclear facilities which used this material as moderator and reflector. In addition to common radiation protection issues, easily volatizing long-lived radionuclides and stored Wigner energy could be released during imprudent retrieval and processing of i-graphite. With this regard, among all cutting technologies, abrasive waterjet (AWJ) can successfully achieve all of the thermo-mechanical and radiation protection objectives. In this work, factorial experiments were designed and systematically conducted to characterize the AWJ processing parameters and the machining capability. Moreover, the limitation of dust production and secondary waste generation has been addressed since they are important aspects for radiation protection and radioactive waste management.

The promising results obtained on non-irradiated nuclear graphite blocks demonstrate the applicability of AWJ as a valid technology for optimizing the retrieval, storage, and disposal of such radioactive waste. These activities would benefit from the points of view of safety, management, and costs.

1. Introduction

Nuclear graphite has been widely used as a neutron moderator and reflector and as a structural material in several nuclear power plant concepts, especially in UK, France, Russian Federation, and USA [1]. So far, more than 250,000 tons of irradiated nuclear graphite (i-graphite) have been generated worldwide and are still waiting for permanent disposal [2]. The large waste inventory and the delays in siting and building deep repositories are not the only reasons which make i-graphite a challenging waste to be managed and which delayed the decommissioning of graphite-moderated nuclear reactors [3]. In fact, the exposure to high neutron fluences (often higher than 10^{22} neutrons/cm^2) produces several effects in the material, such as neutron activation of constituents and impurities, dimensional changes, modification of mechanical properties, and formation of defects leading to the accumulation of Wigner energy [4]. Despite the high purity of nuclear graphite, trace elements do promote important phenomena during irradiation [5–7]. They are mainly activated by neutron fluxes following (n, γ), (n, p) and (n, α) reactions, thus producing a wide range of radionuclides in the graphite matrix, most of them being very volatile or long-lived, such as ^{3}H, ^{14}C and ^{36}Cl. Hence, i-graphite blocks are often classified as intermediate level waste (ILW) and require detailed radiological characterizations before retrieval [8–10]. Over the years, many solutions have been investigated to dismantle and manage i-graphite [11–13]. In most cases, the safe storage has been selected as more convenient decommissioning strategy. This choice was not aimed at reducing the residual radioactivity in the activated graphite blocks, since most activated radionuclides are long-lived, but rather at developing effective pre-disposal processes during the deferred dismantling period [14]. For this purpose, different dismantling and treatment processes have been proposed and studied [15–17]. About these topics, some joint research projects have been funded by the European Commissions or coordinated by the International Atomic Energy Agency (IAEA), like the recently concluded Irradiated Graphite Processing Approaches (GRAPA) project [3,18–20]. Besides the difficulties

* Corresponding author.
E-mail address: eros.mossini@polimi.it (E. Mossini).

https://doi.org/10.1016/j.net.2023.03.026

encountered in identifying the most suited treatment approach, the high operating costs and the lower security of interim storage facilities must be considered [3]. Moreover, some Member States which have operated just a few graphite moderated nuclear power plants or just a few nuclear research reactors are certainly more inclined to postpone the issue of choosing and implementing a definitive i-graphite management approach. In these cases, i-graphite is usually kept for some decades inside the reactor building or, less likely, transferred in temporary repositories, waiting for a final solution. That is also the case of Italy, where, besides a MAGNOX NPP (Latina, Sogin), a L-54 M nuclear research reactor (Milan, Politecnico di Milano) has been shut-down [10]. The decommissioning of both facilities is being managed according to a deferred dismantling strategy, also due to the absence of a national repository for the disposal of the resulting radioactive waste. During the transition period between operation and beginning of dismantling, some activities have been performed to guarantee L-54 M safety and plan the next steps, such as the removal of the spent nuclear fuel and the execution of preliminary radiological characterization. In particular, the focus of this campaign was the irradiated Acheson Graphite Ordinary Temperature (AGOT i-graphite) employed in L-54 M nuclear research reactor as neutron moderator and reflector [6].

The selection of the most appropriate i-graphite waste route depends on its inventory and physical, chemical, mechanical, and radiological properties. Moreover, several technical, economic, strategic, and political issues, among which the seldom defined waste acceptance criteria, should be carefully considered [21]. Nowadays, one of the most accredited options is to extract the whole i-graphite blocks and to either treat or directly dispose them afterwards without any further processing [2,22]. In any case, it may be advantageous to optimize how decommissioned i-graphite waste is placed in a package, to make best use of the available internal space and limit the space occupation in the final repository. To do this several techniques may be employed, such as surface decontamination and cutting. The former is not convenient since radiocontaminants mainly originate from neutron activation, which occurs both in the bulk and on the surface [11], while the latter exploits cutting the i-graphite into blocks so that they can be stored in a more space-efficient way in containers [23]. As i-graphite is usually classified as ILW, this technique would increase the specific activity of the waste package, but without a change of classification. In addition to volatile and long-lived radionuclides content, accumulated Wigner energy is a key issue to be carefully considered when dealing with i-graphite, especially for graphite irradiated at temperatures below 100 °C [1]. In fact, it is sufficient to anneal the material at a temperature of approximately 50 °C higher than the irradiation temperature to release the stored Wigner energy [24]. Consequently, special care must be taken to avoid uncontrolled release of Wigner energy from i-graphite, which may lead to abrupt loss of radionuclides or accidents [25]. In this context, in order to support the next decommissioning operations, the abrasive waterjet (AWJ) cutting technique has been considered, as it could offer several valid advantages over traditional cutting techniques [26–28]. It usually produces small amounts of dusty by-products during cutting and can also be operated under water, which greatly reduces the possibility of dust dispersion [29]. To enhance the radiation protection effectiveness of AWJ technique, remotely-controlled operation can be implemented [30,31]. The combination of low dust production, under water execution and remote-control operation proficiently limits the operational dose received by operators [32]. Another interesting feature, especially from the point of view of Wigner energy release, is the fact that it usually entails limited thermal alteration of the workpiece with respect to conventional mechanical and thermal cutting technologies, *i.e.*, friction-induced heat [33–35]. So far, AWJ technology has been adopted in various manufacturing sectors as a cutting tool for a wide range of materials, such as metals, composites, glass, and ceramics [26,33,36]. The cutting ability of AWJ strongly depends on process parameters and on the physical properties of the processed material. Although the number of significant investigations in the literature is rather small, AWJ technology has already been identified as potential cutting technology for dismantling and cutting operations in nuclear decommissioning [30,31,37]. Moreover, attempts to apply AWJ to the cutting of i-graphite were made, but no results are available in the literature [38].

To the best of the authors' knowledge, a systematic study has not yet been conducted to optimize the AWJ process parameters for i-graphite cutting in view of a potential application in the nuclear decommissioning. This work aims to bridge this gap of knowledge. Non-irradiated AGOT-type graphite blocks from the same manufacturer as those used in L-54 M nuclear research reactor were employed in this study [39]. Factorial experiments were performed using an industrial AWJ cutting machine by varying several process parameters (e.g.: water pressure, abrasive mass flow rate, and traverse velocity) in order to test different experimental conditions, reduce the amount of secondary waste, and identify a suitable processability window. Specifically, the present study investigated the influence of the process parameters on the material removal rate capability of the nuclear grade graphite, in order to estimate the amount of graphite dust that would be collected in the catcher along with the spent abrasive. This information will be required for treating the slurry in the catcher and optimizing the secondary waste management [40,41]. Moreover, the graphite temperature was preliminarily assessed by a temperature sensing system during the cutting process.

2. Materials and methods

2.1. Theoretical background on AWJ cutting

During the process, water is pressurized up to 300–400 MPa through a pressure intensifier, and it is sent to the cutting head, where the primary orifice transforms pressure energy into kinetic energy. Afterwards, the abrasive is mixed to the high-speed water jet to form the AWJ, inside the mixing chamber, Fig. 1.

During the mixing process, a momentum transfer from water to abrasive particles causes their acceleration along the focusing tube [42,43]. Finally, the abrasive jet exits the focusing tube, gets airborne, then interacts on the workpiece producing the material removal. Waterjet velocity v_j Eq. (3) can be obtained from the theoretical velocity v_{th} Eq. (1), that is derived from the Bernoulli equation, considering water compressibility ψ Eq. (2) and irreversibility c_v, respectively [43].

$$v_{th} = \sqrt{\frac{2p}{\rho}} \tag{1}$$

$$\psi = \sqrt{\frac{L}{p(1-n)}\left[\left(1+\frac{p}{L}\right)^{1-n} - 1\right]} \tag{2}$$

$$v_j = c_v \psi \sqrt{\frac{2p}{\rho}} \tag{3}$$

where $L = 300$ MPa and $n = 0.1368$ [42, 43]

Water mass flow rate $\dot{m}_w$ Eq. (4) is obtained from the water density ρ and water volume flow rate Q_w Eq. (5), which in turn can

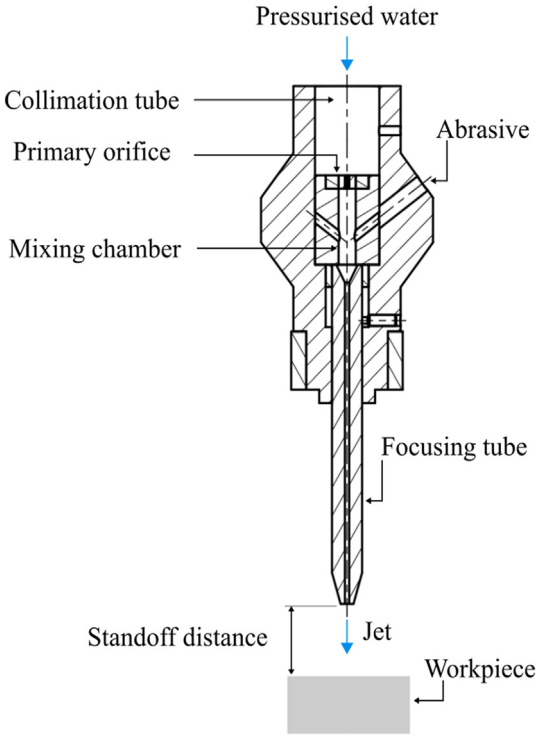

Fig. 1. AWJ head, adapted from Ref. [35] and detail of the cutting kerf geometry.

be calculated from the Bernoulli velocity v_{th}, the nominal cross-sectional area of the orifice S_0, and the orifice discharge coefficient c_d [26,43]. The jet kinetic P_{kin} is defined in Eq. (6).

$$\dot{m}_w = \rho Q_w \tag{4}$$

$$Q_w = c_d S_0 \sqrt{\frac{2p}{\rho}} \tag{5}$$

$$P_{kin} = \frac{1}{2}\dot{m}_w v_j^2 \tag{6}$$

As soon as the waterjet enters the mixing chamber (Fig. 1), it starts mixing with the incoming abrasive particles, which are pneumatically delivered to the mixing chamber. During the mixing process, which starts in the mixing chamber and continues inside the focusing tube, momentum transfer from water to abrasive particles happens. To this purpose, the abrasive loading ratio r_d (Eq. (7)) is introduced to explain the momentum transfer from the water to the abrasive particles. The mixed jet velocity v_{abr} (Eq. (8)) depends on r_d. v_{abr} is the equilibrium velocity of the mixed jet, which is composed by water, abrasive particles, and air when it exits from the focusing tube, under the hypothesis of no energy losses in the mixing process. Finally, it is possible to express the kinetic power of the abrasive particles (from now on, it will be called jet power), P_{part} as the only portion of the kinetic power of the AWJ that is useful for the material removal process(Eq. (9)) [42].

$$r_d = \frac{\dot{m}_a}{\dot{m}_w} \tag{7}$$

$$v_{abr} = \frac{v_j}{1 + r_d} \tag{8}$$

$$P_{part} = \frac{1}{2}\dot{m}_a v_{abr}^2 \tag{9}$$

According to Hashish [42], the jet power P_{part} is related to the material removal rate of the process, *i.e.*, the amount of removed material per unit of time. For this reason, P_{part} is the physical quantity better representing the jet cutting capability [42,44–46].

During the cutting process, not all the jet power is spent for the material removal. In fact, a series of physical phenomena have been observed during AWJ cutting, among them vibroacoustic emission [44,47–53] and thermal emission [54–57]. According to Refs. [33,57], a fraction of the abrasive particles kinetic power (P_{part}) is converted into thermal power, which is responsible for the workpiece temperature increase during the cutting process.

Experimental results reported in Refs. [55,56,58] showed how, on average, the measured maximum temperature was below 70 °C. However, Kovacevic et al. [56] detected water vapor during AWJ cutting of materials like titanium, as a consequence of localized heating effects. Such effects may constitute a risk in highly thermal sensitive materials like the irradiated nuclear graphite.

2.2. Samples preparation and sensing system

The herein reported experiments have been conducted on fourteen squared blocks of non-irradiated graphite prepared starting from a 600 mm × 100 mm x 100 mm AGOT-type rod, through sawing operation. It belongs to the same stock employed as reflector and moderator at L-54 M nuclear research reactor, operated between 1959 and 1979 at Politecnico di Milano, Italy [39]. So far, in order to develop an accurate neutron activation model in support of the radiological characterisation, great efforts have already been made to determine the elemental composition of AGOT used in L-54 M reactor [7,59]. Some physical properties of the AGOT-type graphite are reported in Table 1.

Each block dimensions were: 30 mm × 100 mm x 100 mm. Afterwards, twelve 1 mm diameter blind holes, were drilled on each graphite block by mechanical drilling, six for each side, as reported in Fig. 2. The purpose of each hole was to host a thermocouple to measure the temperature during the cutting process. To avoid any collisions between the moving AWJ and each thermocouple, each of these were placed at 5 mm far from the centre line of the cutting path (Fig. 2). For this reason, the drilling depth of each blind hole was 10 mm.

Each sample was instrumented with twelve k-type thermocouples (IEC 60584), (Tersid, Milan, Italy). The instrumented graphite sample is shown in Fig. 3 where the setup components are visible.

The experimental activity was conducted using a CNC (Computerized Numerical Control) AWJ cutting machine (IDRO 1740, CMS SpA, Zogno, Italy), with a double effect high pressure intensifier pump (Flow International Corporation). A pressure

Table 1
AGOT-type graphite properties [59].

Property	Value
Bulk density (g•cm^{-3})	1.69 ± 0.03
Skeletal density (g•cm^{-3})	2.29 ± 0.02
Porosity (%)	26.4 ± 0.7
Thermal conductivity (W•m^{-1}•K^{-1})	166
Specific heat capacity (J•kg^{-1}•K^{-1})	760

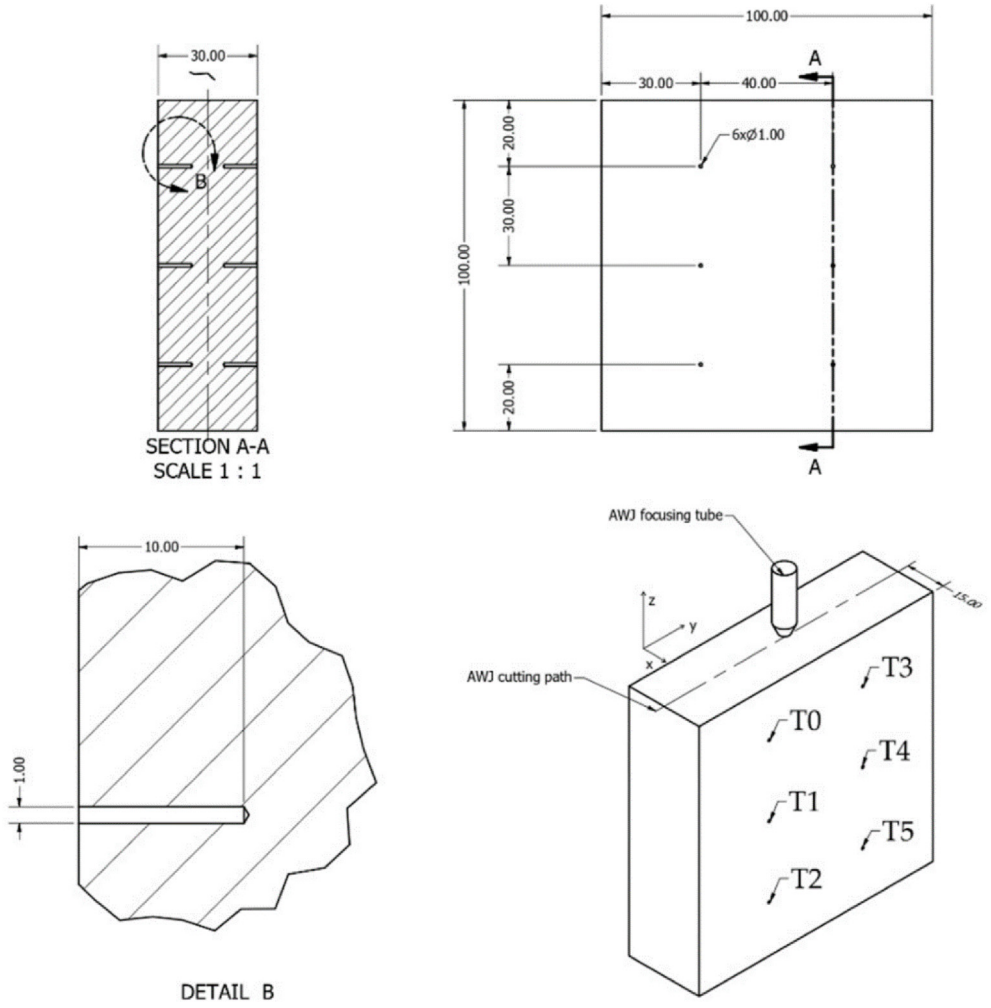

Fig. 2. Graphite samples dimensions and detail of the blind holes (all dimensions are in mm).

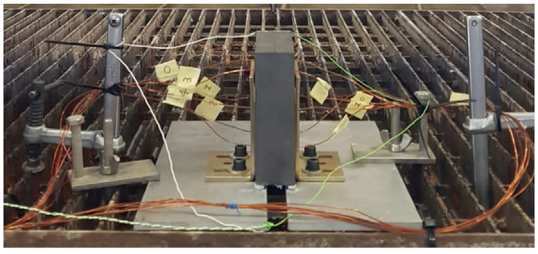

Fig. 3. Sensing system.

gauge was mounted at the pressure intensifier outlet to measure water pressure in every experimental run. The abrasive mass flow rate was regulated by an abrasive feeding system. Detail of the AWJ cutting head and abrasive feeding system is reported in Fig. 4.

In this study, GMA GARNET (Australian GMA Garnet), mesh# 80, was used as abrasive powder. It is composed of silicates and is extracted from mines. Chemical and mineralogical composition of the employed abrasive was provided by the vendor and is reported in Table 2.

2.3. Experimental design and data analysis method

The experiments consisted in a series of cutting tests that were performed in one single pass on AGOT-type graphite samples. For each experimental run, the sample was held in place, as shown in Fig. 3, while the AWJ cutting head was moved according to a specific traverse velocity, which was set through the CNC system. The aim of the experiment was to investigate the material removal rate, as well as the graphite temperature during the cutting process. The following process parameters were considered.

- Water pressure, p (MPa);
- Abrasive mass flow rate, $\dot{m}_a$ (g•min^{-1});
- Traverse velocity, v_f (mm•min^{-1});

Table 3 summarizes all the process parameters that were considered for the design of the experiment. Both variable and constant parameters are reported.

The levels defined for each variable parameter, were identified through a screening experiment based on a DOE (Design Of Experiment) methodology. The screening experiment consisted in a series of cutting experiments of 100 mm thick graphite block. The objective aimed at finding a suitable processability window, *i.e.* the region of process parameters producing a complete-separation cut on the 100-mm-thick AGOT-type graphite bar. The screening experiment

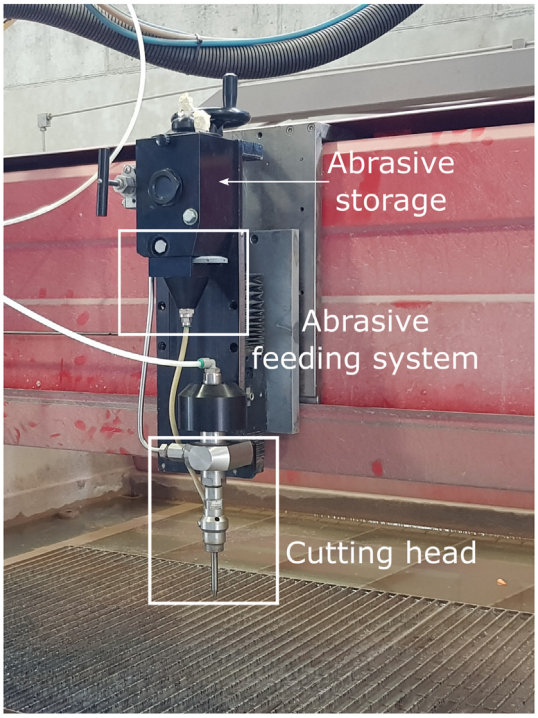

Fig. 4. AWJ cutting apparatus: detail of the abrasive feeding system; high pressure water line; cutting head.

Table 2
Chemical composition of the Garnet abrasive.

Chemical name	Symbol	Proportion (weight%)
Almandine Garnet	$Fe_3Al_2(SiO_4)_3$	>97
Ilmenite	$FeTiO_3$	<2.0
Calcium Carbonate	$CaCO_3$	<1.5
Zircon	$ZrSiO_4$	<0.2
Quartz	SiO_2	<0.2

Table 3
Constant parameters and variable factors.

Fixed parameters	**Values**
Standoff distance, *sod* (mm)	3
Thickness, t (mm)	100
Primary orifice diameter, d_n (mm)	0.33
Focusing tube diameter, d_f (mm)	1.02
Focusing tube length, l_f (mm)	75
Type of abrasive	Barton Garnet
Abrasive mesh number	80
Variable parameters	**Values**
Water pressure, p (MPa)	125–280
Abrasive mass flow rate, $\dot{m}_a$ (g•min^{-1})	170–480
Traverse velocity, v_f (mm•min^{-1})	20–40

showed how the AWJ cutting capability strictly depends on the ratio between the jet power and the traverse velocity. In particular, each combination of water pressure (100 MPa $\leq p \leq$ 380 MPa), abrasive mass flow rate (50 g • min^{-1} $\leq \dot{m}_a \leq$ 480 g • min^{-1}), traverse velocity (20 mm • min^{-1} $\leq v_f \leq$ 300 mm • min^{-1}) which yields $P_{part}/v_f > 225$ J • mm^{-1} was sufficient to obtain a separation cut.

Even if a separation cut is obtained, the quality of the width of a cut could be poor. However, an acceptable level of quality would be fundamental to ensure a better mechanical coupling of the segmented graphite blocks during the confinement process. For this reason, the levels of the variable parameters of the experimental plan were determined starting from a value of $P_{part}/v_f > 550$ J • mm^{-1}, which experimentally resulted in an acceptable cutting quality for the process.

The selected control factors of the experimental plan were the jet power (P_{part}) and the traverse velocity (v_f), which is the traverse speed of the cutting head, and it is related to the productivity of the process. P_{part} is the source of mechanical power that is partially converted into thermal power during the cutting process. Indeed, the jet power is related to the material removal rate. For these reasons, it was reasonable to assume the jet power as a control factor of the experimental design. As defined in Eq. (9), P_{part} depends on both water pressure p and the abrasive mass flow rate $\dot{m}_a$. These two process parameters were combined to generate different levels of P_{part}.

A central composite design (CCD) scheme was selected to setup a proper experimental design to handle potential linear, quadratic and interaction terms in the empirical modelling of the response variables [60,61]. A CCD is composed by corner points ($n_F = 2^k$), axial points ($n_a = 2k$) and center points (n_c) as shown in Fig. 5, where k is the number of control factors of the experimental plan, *i.e.* k = 2.

For a two-factor CCD, the distance between the axial points and the centre point, named α (Fig. 5), must be accurately selected. The choice of α depends on the number of corner points as $\alpha = n_F^{1/4} = \sqrt{2}$, [61]. The values of the control factors are reported in Table 4.

Coded variables are useful to compare the weight of factor effects on response variables [60,61]. Eq. (12) and Eq. (13), reported below, were used to obtain coded variables' values:

$$P^*_{part} = \frac{2\left(P_{part} - P^{cp}_{part}\right)}{P^H_{part} - P^L_{part}} \tag{12}$$

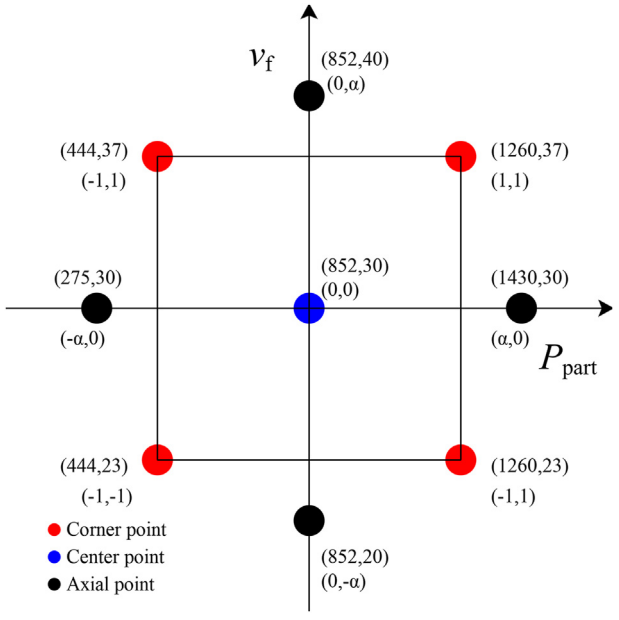

Fig. 5. Central composite design (CCD) scheme for two control factors of the experimental plan (adapted from Ref. [60]), in both natural and coded units.

Table 4
Control factors levels of the experimental design.

Control factor	Lower axial point	Higher axial point	Lower corner point (L)	Higher corner point (H)	Center (cp)
P_{part} (W)	275	1430	444	1260	852
v_f (mm•min^{-1})	20	40	23	37	30

$$v_f^* = \frac{2\left(v_f - v_f^{cp}\right)}{v_f^H - v_f^L} \quad (13)$$

where the superscript * stands for the coded units, cp stands for the center point, H and L stand for higher and lower corner point, respectively (Table 4).

The center point was replicated six times, while both the corner points and axial points were replicated once, as suggested in Ref. [61]. The total number of experimental runs was fourteen. The material removal rate (MRR) was also investigated. To this purpose, the formula reported in Eq. (12) was used, where l_c is the length of the cutting path (100 mm), m_f and m_i are the dried sample mass after and before the cutting experiment. To this purpose, each sample was dried in an industrial oven at a controlled temperature of 115 °C for 48 h before and after each cutting operation.

$$MRR = \frac{m_f - m_i}{l_c} v_f \quad (14)$$

Each sample mass was measured using an analytical balance. For each experimental run, once the AWJ cutting machine had been started, the temperature was measured by means of the thermocouples placed inside each graphite sample (Fig. 3).

The data analysis was performed according to the following steps.

1. For each experimental run, the material removal rate was calculated, and the value of the maximum temperature was registered.
2. Exploratory graphical analysis: material removal rate data were represented according to the main effect plots, to visually investigate the most influential effects of the control factors.
3. In order to develop an empirical model of material removal rate (MRR), data were fitted with a full quadratic model (Eq. (15)):

$$y = \beta_0 + \sum_{i=1}^{k} \beta_i x_i + \sum_{i=1}^{k} \beta_{ii} x_i^2 + \sum_{i<j} \sum \beta_{ij} x_i x_j + \varepsilon \quad (15)$$

where the coefficients of the model were found using the least squares method. The significance of the model was tested using the analysis of variance (ANOVA).

3. Results and discussion

The calculated MRR together with the measured total mass of material removed Δm for each set of inputs is reported in Table 5.

Fig. 6 shows the effect of control factors, P_{part} and v_f on the MRR.

Both control factors have a positive effect on the MRR, as predicted by the theory of AWJ material removal rate [26,43]. MRR linearly increases with the traverse velocity, as well as with the AWJ power, as stated by Hashish's model [42,43]. The material removal rate data have been fitted with a second order polynomial response surface. ANOVA was performed to look for significant effects of the full quadratic model. Three terms were found to exhibit more evident significance in the model (p-value <0.05): first order term of jet power (P_{part}), second term of jet power (P_{part}^2) and first order term of traverse velocity (v_f). Finally, a reduced model was fitted, including all significant factors. Estimated coefficients and their standard errors are shown in Table 6 for the MRR model.where, P_{part} is the jet power (W), v_f is the traverse velocity (mm•min^{-1}), MRR (g•s^{-1}) is the material removal rate. The fundamental assumptions of the linear regression analysis were tested. Model adequacy was checked considering the normality of the standardized residuals. Standardized residuals do not show any apparent pattern against fitted values. The model adequacy checking did not find any influential observations (Cook's distance: $D \leq \pm 1$), as well as any significant collinearity between predictors. Indeed, in Fig. 6, the total removed mass Δm is plotted against the traverse velocity to investigate the potential effect of the said parameter on the dust formation during the cutting process. However, results do not show any evident correlation between the total removed mass and the traverse velocity (p-value = 0.1846). Fig. 7 shows the contour plot of the calculated response surface material removal rate as a function of the control factors P_{part} and v_f. Statistical analysis supports the experimental results, for which an increase of either the jet power (i.e., water pressure and/or abrasive mass flow rate) or the traverse velocity, increases the material removal rate.

Table 5
Measured MRR (g/s) and total mass of material removed Δm (g) for each experimental run.

Run order	P_{part}	v_f	Δm	*MRR* (J•mm-1)
1	444	37	36	0.22
2	444	23	39	0.15
3	1260	23	51	0.19
4	852	30	42	0.21
5	1260	37	45	0.28
6	852	30	44	0.22
7	852	30	43	0.22
8	275	30	32	0.16
9	852	30	43	0.22
10	852	30	43	0.22
11	852	40	40	0.27
12	852	30	43	0.22
13	1430	30	49	0.25
30	852	20	47	0.16

Finally, temperature data have been graphically represented in Fig. 8, according to the x and y coordinates of the measuring sensor. The highest temperature has been measured in the upper part of the graphite sample, which is closer to the jet entrance and therefore receives higher mechanical power. In fact, the jet loses its power as it cuts through the target sample, then the fraction of mechanical power transformed into heat power decreases with depth.

Several countermeasures could be undertaken to meet the different radiation protection requirements which could be imposed by a safety authority. Reasonably, it may be asked to limit the dose delivered to the workers; limit the radioactivity discharge that could hamper the public – including the future generations – and the environment; reduce the volumes of secondary waste to be disposed, and, in general, consider safety, security, social, and economic requirements [62,63]. The safeguard of workers' health could be pursued thanks to the possibility of implementing remotely-controlled and under water operation of the AWJ

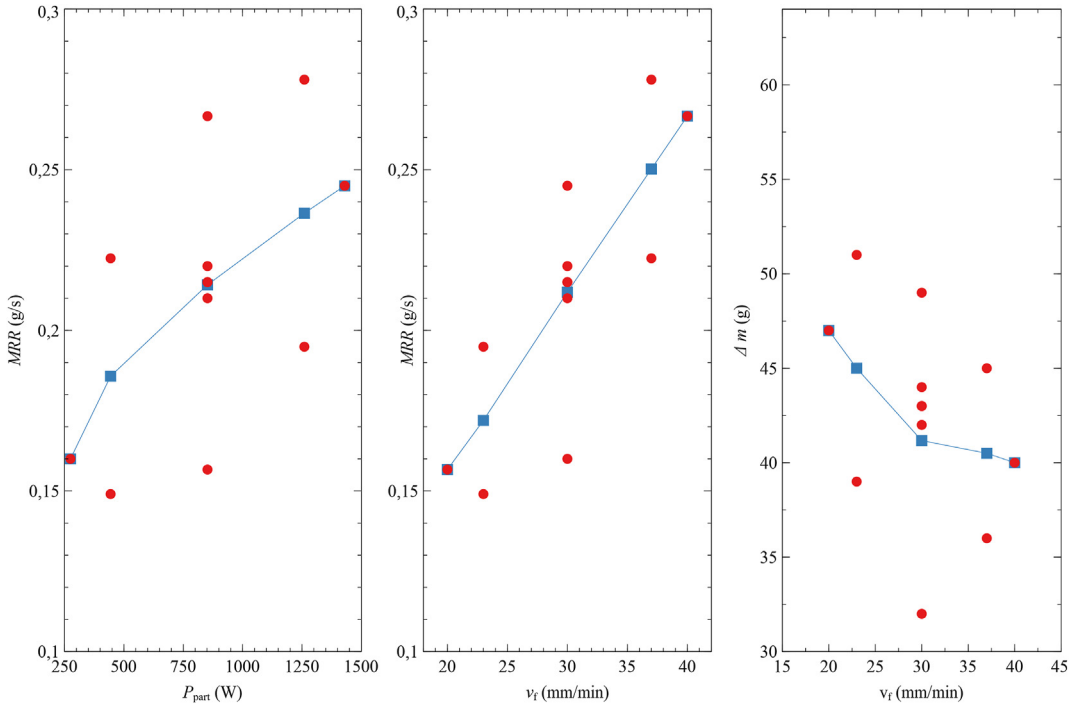

Fig. 6. Effect of the control factors on the MRR. Left panel: power effect. Right panel: traverse velocity effect. The red circles represent the experimental points, while the black squares represent the average values.

Table 6
Estimated coefficients of the response surface model for MRR.

$$MRR = -3.227 \bullet 10^{-2} + 1.211 \bullet 10^{-4} P_{part} + 5.545 \bullet 10^{-3} v_f - 3.124 \bullet 10^{-8} P_{part}^2 \quad (16)$$

Coefficient	Estimate	Std. Error	t-value	p-value
Constant	−3.227e-02	8.611e-03	−3.748	0.00380
P_{part}	1.211e-04	1.511e-05	8.019	1.15e-05
v_f	5.545e-03	1.971e-04	28.129	7.49e-11
P_{part}*P_{part}	−3.124e-08	8.634e-09	−3.618	0.00471

A regression equation for MRR ($R^2_{adj} = 0.9896$) is reported in Eq. (14).

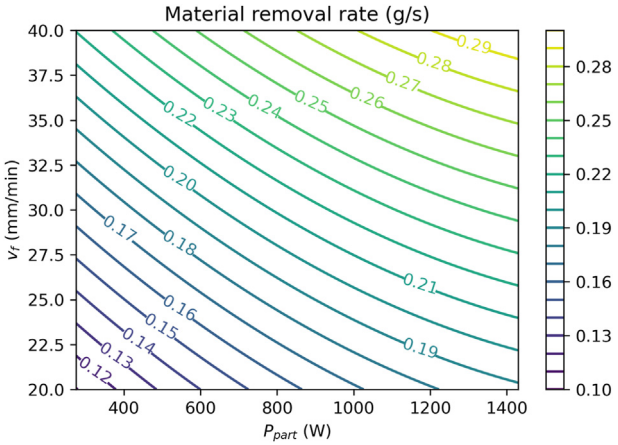

Fig. 7. Contour plot of the MRR response surface (Eq. (14)).

equipment. Beside strongly reducing the dose that operators directly receive from the i-graphite blocks undergoing cutting operations, also the suspended dust particles would be abated, reducing the inhalation risk, and allowing to simplify the air filtration system [30,32]. In addition, the discovery of a process-ability window allows to select the optimal AWJ working conditions that could help in satisfying radiation protection and waste management requirements. Above all, the temperature increase in the block must be carefully controlled while handling i-graphite to avoid the undesired discharge of Wigner energy [1]. Besides, the material warming would most likely favour the release of volatile radionuclides (such as tritium, Cl-36, and the more easily mobilised fraction of C-14) from the surface, which would hamper not only the worker's health, but also the safety of the public and the environment [13,23]. The mitigation of radionuclides dispersion requires the implementation of defence in depth approach, e.g. by confining the working area, operating dust abatement and air filtration system [64]. To further improve the safety of the decommissioning operations, the AWJ cutting could be operated under water to limit the dispersion of volatile radionuclides in the air. The contaminated process water may be reused several times to avoid the excessive production of radioactive secondary waste. Afterwards, the effluent would be managed as radioactive waste. Since 50 °C is the maximum temperature increment that would not endanger the i-graphite blocks from a Wigner energy perspective, a wide range of process parameters values could be selected. In fact, as shown in Fig. 8, the safety requirement is satisfied by all the tested combinations of the process parameters that allow a separation cut. Hence, the choice of the optimal process parameters for i-graphite cutting is not limited by temperature constraints. For this reason, it could be driven by other safety criteria.

It is worth noting that impurities activation and Wigner energy storage are not the only effects induced by fast neutron irradiation, thermal and radiolytic oxidation. Dimensional changes, modification of mechanical strength and thermal conductivity occur on i-graphite [65]. The magnitude of these alterations depends on several parameters, such as neutron fluence, irradiation

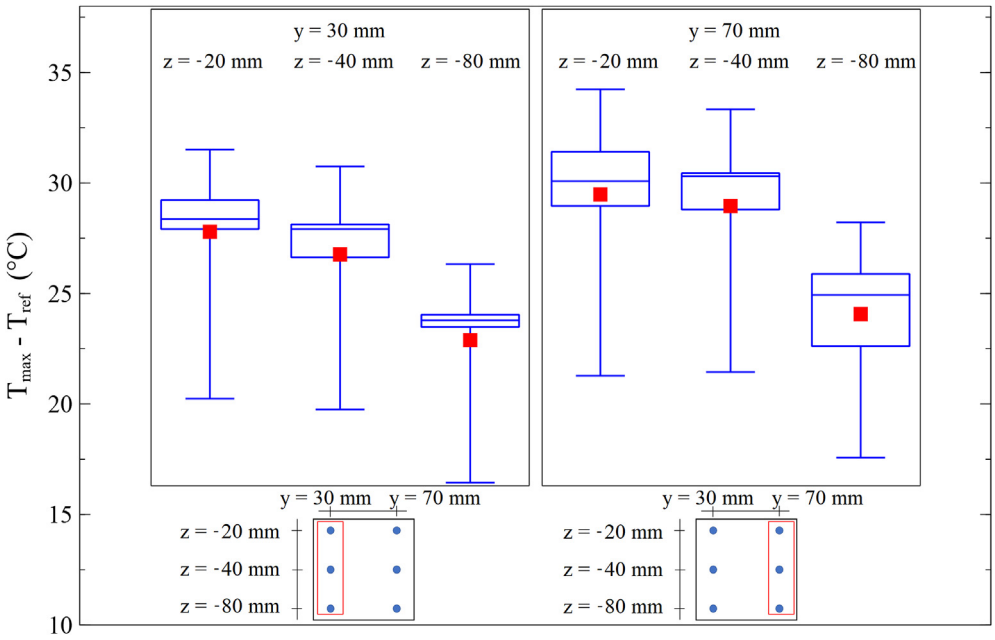

Fig. 8. Measured peak temperatures at different referenced coordinates inside the samples. Red squares represent the averages values.

temperature, virgin graphite properties, coolant gas pressure and composition [1]. Hence, it is difficult to *a priori* envisage how the cutting performance would be affected in the case of i-graphite. The processability window should be verified on a case-by-case basis. In general, at high doses mechanical strength and thermal conductivity decrease, while porosity increases. Therefore, with respect to virgin graphite, the cutting would probably become easier, but the heat dissipation would worsen. Although this last issue would affect all cutting technologies, it could be successfully mitigated by operating the AWJ cutting under water.

A relevant aspect from the perspective of waste management is the limitation of the material removal rate (MRR). Besides being radioactive, the irradiated graphite contains easily volatilising radionuclides that could be released during the cutting operations, especially when the material is pulverised or slightly heated. Such radionuclides could dissolve in the process water and accumulate in the catcher, or disperse in the atmosphere, thus endangering workers and public health if not properly addressed. As shown in Fig. 7, by duly choosing the working conditions within the processability window a successful cut could be obtained, while at the same time limiting the MRR. The pulverised i-graphite should then be properly managed to ensure its safe disposability. An option could be recovering it from the catcher, separating it from the spent abrasive (e.g. by the different density) that could be recycled, and encapsulating the recovered i-graphite following the so-called "mortar and concrete" strategy [3]. At this stage, the contaminated water could be used as mixing water for the production of the cementitious matrices. Another important issue is the reduction of the secondary waste that will be unavoidably produced since it will require proper management to be safely disposed of. Besides the i-graphite dust, the secondary waste includes the spent abrasive material. Originally this is not radioactive, but it will come in contact with radionuclides and become contaminated during the cutting process. As reported, the abrasive mass flow rate may be reduced and still a successful cut could be obtained.

The graph in Fig. 7 can be used to operate into a particular target of primary waste production (i.e., the amount of removed graphite during the cutting process) that is considered sufficiently safe. In the same way, the process parameters can be selected to limit the secondary waste (abrasive) by increasing the water pressure.

For example, considering the case where MRR target level is 0.135 g/s, the corresponding cutting capacity can be achieved with a traverse velocity of 25 mm/min (intermediate cutting quality level). Therefore, it would result $P_{part} \cong 275$ W. Finally, the process parameters can be retrieved from the jet power value (Eq. (1) - Eq. (1)(9). One of the possible combinations of process parameters, inside the experimental range, which satisfy all requirements is: water pressure ($p = 125$ MPa) and the abrasive mass flow rate ($\dot{m}_a = 0.17$ kg/min). The selected operative specifications would lead to a secondary waste production rate of 1.78 kg/min, of which 1.61 kg/min of water. Said flow rate was calculated from Eq. (4), while the total graphite removed mass rate was 8.1 g/min.

The reduction of the amount of the abrasive would not just limit the secondary waste production and ease its management, but also reduce the cost of the cutting process. An option could be retrieving the solid residues from the tank to recycle the water, without discriminating between the pulverised i-graphite and the spent abrasive, and encapsulate them by using a cement binder, following the mortar and concrete approach. In fact, it is not recommended to recycle the spent abrasive powder because its cutting capability would be reduced after some cutting cycles [66]. The cementation approach would be straightforward and easily applicable. Besides the encapsulation of i-graphite in concrete, also the spent abrasive can be proficiently conditioned, even allowing to improve mechanical resistance and durability of the matrix [67].

The transferability of the AWJ to reactor dismantling needs to accomplish different challenges such as the cutting of very thick materials that can be done either in situ or ex situ. In situ dismantling involves cutting and removing materials while they are still in the reactor. This approach can be advantageous in terms of minimizing the amount of waste generated, reducing the need for heavy lifting equipment, and simplifying the handling and disposal of radioactive materials. However, in situ dismantling can be more complex and time-consuming, as it requires working in a confined and often highly radioactive environment. According to Hashish, a few approaches can be used to cut very tick materials

(>50 mm–600 mm) [68]. The most significant one consists of a multi pass cutting strategy in which an oscillating AWJ cutting head passes several times to groove into the material. For each pass the standoff distance is adjusted in order to keep it as much as constant. Said method was experimented to cut through nuclear grade reinforced concrete, resulting in a 0.5–1.0 m^2/h cut area rate. Indeed, vacuum systems can be useful for in-situ dismantling. During the process, the removed material is sucked up and transported to a separate containment vessel for further processing and disposal. The vacuum system can be designed to work in conjunction with the waterjet cutting system. Preliminary experimental results reported that cuttings and water were 80% contained using a unique vacuum system [68].

4. Conclusions

In this paper, the applicability of the AWJ to i-graphite cutting was evaluated. One of the objectives of the paper was to investigate the effect of the process parameters on the temperature of the graphite during the cutting process. This is essential to assess whether this type of technique can also be used for cutting irradiated graphite at low temperatures to avoid Wigner energy release.

The experiments showed that the temperature variation in the case of 100 mm thick, AGOT-type virgin nuclear graphite does not exceed the 50 °C limit. The maximum temperature increase was lower than 35 °C. Results demonstrated that AWJ cutting may be a valuable cutting process for the segmentation of the irradiated graphite. For this reason, further studies are needed to validate the processability window and to estimate the maximum temperature during the cutting of irradiated graphite blocks, therefore when thermal conductivity is expected to worsen. The MRR was measured in order to investigate the overall volume of secondary waste produced by the cutting process. A good agreement between theory and experiments has been found since both the AWJ kinetic power and the traverse velocity were found to be significant for the MRR. A quadratic regression model has been developed, in which the traverse velocity exhibits a positive effect on the MRR, whilst the jet power showed a quadratic effect on the material removal rate.

The secondary waste could be proficiently managed by recycling the water in the tank, while recovering both spent abrasive and i-graphite from the tank to be then encapsulated in cementitious matrices or, preferably, in a more sustainable and durable geopolymer.

As a further study, it would be interesting to better investigate the possibility of conducting underwater cutting experiments. In fact, this almost eliminates the possibility of splashing, while the amount of dust produced during cutting, which is usually already very low in this type of technique, may be further reduced. From a point of view of an industrial application and radiation protection, the underwater cutting strategy would further limit the radiation dose, because of the shielding action of water, reduce the dispersion of volatile radionuclides, and improve the heat dissipation, thus increasing the safety of the process. Another advantage of the underwater cut could be to reduce the maximum peak temperature. In fact, by immersing the graphite blocks in water, the heat would be quickly dissipated as water has a higher convective heat exchange coefficient than air.

Sample CRediT author statement

Francesco Perotti: Investigation, Methodology, Formal analysis, Writing - Original Draft; **Eros Mossini:** Conceptualization, Data curation, Writing - Original Draft; **Elena Macerata:** Visualization, Writing - Review & Editing; **Massimiliano Annoni:** Resources, Supervision, Writing - Review & Editing; **Michele Monno:** Resources, Supervision.

Declaration of competing interest

The authors declare that they have no known competing financial interests or personal relationships that could have appeared to influence the work reported in this paper.

References

[1] Characterization, Treatment and Conditioning of Radioactive Graphite from Decommissioning of Nuclear Reactors, IAEA, 2006.
[2] Processing of Irradiated Graphite to Meet Acceptance Criteria Got Waste Disposal : Results of a Coordinated Research Project, International Atomic Energy Agency, Vienna, Austria, 2016.
[3] A. Wickham, H.J. Steinmetz, P. O'Sullivan, M.I. Ojovan, Updating irradiated graphite disposal: project 'GRAPA' and the international decommissioning network, J. Environ. Radioact. 171 (2017), https://doi.org/10.1016/j.jenvrad.2017.01.022.
[4] I.A.E. Agency, Progress in Radioactive Graphite Waste Management, International Atomic Energy Agency (IAEA), 2010. http://inis.iaea.org/search/search.aspx?orig_q=RN:42052519.
[5] R. Plukiene, E. Lagzdina, L. Juodis, A. Plukis, A. Puzas, R. Gvozdaite, V. Remeikis, Z. Révay, J. Kučera, D. Ancius, D. Ridikas, Investigation of impurities of RBMK graphite by different methods, Radiocarbon 60 (2018), https://doi.org/10.1017/RDC.2018.93.
[6] R. Takahashi, M. Toyahara, S. Maruki, H. Ueda, T. Yamamoto, Investigation of Morphology and Impurity of Nuclear Grade Graphite, and Leaching Mechanism of Carbon-14, Nuclear Graphite Waste Management Technical Committee Meeting, 2001.
[7] E. Mossini, Z. Revay, A. Camerini, M. Giola, G. Magugliani, E. Macerata, M. Mariani, Determination of nuclear graphite impurities by prompt gamma activation analysis to support decommissioning operations, J. Radioanal. Nucl. Chem. 331 (2022) 3117–3123, https://doi.org/10.1007/s10967-022-08381-3.
[8] C. Fréchou, J.P. Degros, Radiological inventory of irradiated graphite samples, J. Radioanal. Nucl. Chem. 273 (2007), https://doi.org/10.1007/s10967-007-0930-6.
[9] X. Hou, Rapid analysis of 14C and 3H in graphite and concrete for decommissioning of nuclear reactor, Appl. Radiat. Isot. (2005) 62, https://doi.org/10.1016/j.apradiso.2005.01.008.
[10] E. Mossini, L. Codispoti, G. Parma, F.M. Rossi, E. Macerata, A. Porta, F. Campi, M. Mariani, MCNP model of L-54M nuclear research reactor: validation by preliminary graphite radiological characterization, J. Radioanal. Nucl. Chem. 322 (2019), https://doi.org/10.1007/s10967-019-06913-y.
[11] K. Fu, M. Chen, S. Wei, X. Zhong, A comprehensive review on decontamination of irradiated graphite waste, J. Nucl. Mater. 559 (2022), https://doi.org/10.1016/j.jnucmat.2021.153475.
[12] J. Fachinger, W. von Lensa, T. Podruhzina, Decontamination of nuclear graphite, Nucl. Eng. Des. 238 (2008) 3086–3091, https://doi.org/10.1016/j.nucengdes.2008.02.010.
[13] J. Li, M. lou Dunzik-Gouga, J. Wang, Recent advances in the treatment of irradiated graphite: a review, Ann. Nucl. Energy 110 (2017), https://doi.org/10.1016/j.anucene.2017.06.040.
[14] I.A.E. Agency, Selection of Decommissioning Strategies: Issues and Factors Report by an Expert Group, International Atomic Energy Agency (IAEA), 2005. http://inis.iaea.org/search/search.aspx?orig_q=RN:37026187.
[15] E.v. Bespala, M.v. Antonenko, D.O. Chubreev, A.v. Leonov, I.Y. Novoselov, A.P. Pavlenko, V.N. Kotov, Electrochemical treatment of irradiated nuclear graphite, J. Nucl. Mater. 526 (2019), https://doi.org/10.1016/j.jnucmat.2019.151759.
[16] A. Theodosiou, A.N. Jones, D. Burton, M. Powell, M. Rogers, V.B. Livesey, The complete oxidation of nuclear graphite waste via thermal treatment: an alternative to geological disposal, J. Nucl. Mater. 507 (2018), https://doi.org/10.1016/j.jnucmat.2018.05.002.
[17] G. Wei, Y. Miao, B. Yuan, X. Lu, Investigation of the mechanism for simulated graphite waste treatment via microwave sintering technology, J. Hazardous Mater. Lett. 2 (2021), https://doi.org/10.1016/j.hazl.2021.100046.
[18] S. Norris, M. Capouet, Overview of CAST project, Radiocarbon 60 (2018), https://doi.org/10.1017/RDC.2018.142.
[19] M.P. Metcalfe, A.W. Banford, H. Eccles, S. Norris, EU Carbowaste project: development of a toolbox for graphite waste management, J. Nucl. Mater. 436 (2013), https://doi.org/10.1016/j.jnucmat.2012.11.016.
[20] M.I. Ojovan, A.J. Wickham, Processing of irradiated graphite: the outcomes of an IAEA coordinated research project, MRS Adv. (2016), https://doi.org/10.1557/adv.2017.198.
[21] L. Abrahamsen-Mills, A. Wareing, L. Fowler, R. Jarvis, S. Norris, A. Banford, Development of a multi criteria decision analysis framework for the assessment of integrated waste management options for irradiated graphite, Nucl. Eng. Technol. 53 (2021) 1224–1235, https://doi.org/10.1016/

J.NET.2020.10.008.
[22] G. Canzone, R. lo Frano, M. Sumini, F. Troiani, Dismantling of the graphite pile of Latina NPP: characterization and handling/removal equipment for single brick or multi-bricks, Prog. Nucl. Energy 93 (2016), https://doi.org/10.1016/j.pnucene.2016.08.010.
[23] A. Wareing, L. Abrahamsen-Mills, L. Fowler, M. Grave, R. Jarvis, M. Metcalfe, S. Norris, A.W. Banford, Development of integrated waste management options for irradiated graphite, Nucl. Eng. Technol. 49 (2017), https://doi.org/10.1016/j.net.2017.03.001.
[24] R.H. Telling, M.I. Heggie, Radiation defects in graphite, Phil. Mag. 87 (2007), https://doi.org/10.1080/14786430701210023.
[25] R. Wakeford, The Windscale reactor accident - 50 Years on, J. Radiol. Prot. 27 (2007), https://doi.org/10.1088/0952-4746/27/3/E02.
[26] M.P.G. Annoni, M. Monno, C. Ravasio, Water Jet, a Flexible Technology, Polipress, 2007.
[27] D. Krajcarz, Comparison Metal Water Jet Cutting with Laser and Plasma Cutting, in: Procedia Eng, 2014, https://doi.org/10.1016/j.proeng.2014.03.061.
[28] G.R. Lee, B.J. Lim, D.W. Cho, C.D. Park, Selection methodology of the optimal cutting technology for dismantling of components in nuclear power plants, Ann. Nucl. Energy 166 (2022), https://doi.org/10.1016/j.anucene.2021.108808.
[29] Y. Nakamura, K. Sano, Y. Morishita, S. Maruyama, S. Tezuka, D. Ogane, Y. Takashima, The study on abrasive water jet for predicting the cutting performance and monitoring the cutting situation in the water, J. Eng. Gas Turbines Power 133 (2011), https://doi.org/10.1115/1.4002252.
[30] L. Denissen, L. Ooms, H. Davain, Remote high pressure water jet cutting used at the BR3 nuclear dismantling site, in: 17th International Conference on Water Jetting: Advances and Future Needs, 2004.
[31] H. Louis, D. Peter, F. Pude, R. Versemann, Flexible and mobile abrasive waterjet cutting system for dismantling applications, in: WJTA American Waterjet Conference 2005 (13th), 2005.
[32] K.S. Jeong, S.K. Park, I.H. Hahm, J.H. Ha, S.J. Min, S.B. Hong, B.K. Seo, B. Lee, D.H. Kim, J.H. Kim, S.Y. Jeong, S.M. Ahn, J.J. Lee, B.S. Lee, Approach to optimization of risk assessment based on an evaluation matrix for decommissioning processes of a nuclear facility, Ann. Nucl. Energy 128 (2019), https://doi.org/10.1016/j.anucene.2018.12.049.
[33] A.W. Momber, R. Kovacevic, Principles of Abrasive Water Jet Machining, first ed., Springer London, London, 1998 https://doi.org/10.1007/978-1-4471-1572-4.
[34] S. Schmolke, F. Pude, L. Kirsch, M. Honl, K. Schwieger, S. Krömer, Temperature measurements during abrasive water jet osteotomy, Biomed. Tech. 49 (2004), https://doi.org/10.1515/bmt.2004.004.
[35] J.A. McGeough, Cutting of food products by ice-particles in a water-jet, in: Procedia CIRP, 2016, https://doi.org/10.1016/j.procir.2016.03.009.
[36] M. Annoni, F. Arleo, F. Viganò, Micro-waterjet technology, in: Micro-Manufacturing Technologies and Their Applications, Springer, 2017, pp. 129–148.
[37] M. Tezuka, Y. Nakamura, H. Iwai, K. Sano, Y. Fukui, The development of thermal and mechanical cutting technology for the dismantlement of the internal core of Fukushima Daiichi NPS, J. Nucl. Sci. Technol. 51 (2014), https://doi.org/10.1080/00223131.2014.912969.
[38] D. Holland, U. Quade, F.W. Bach, P. Wilk, A German Research Project about Applicable Graphite Cutting Techniques, 2001.
[39] R.E. Nightingale, Nuclear Graphite: Prepared under the Auspices of the Division of Technical Information united states Atomic Energy Commission, Academic press, 2013. https://books.google.co.uk/books?id=qMg3BQAAQBAJ.
[40] M. Harada, I. Yokota, K. Nishi, K. Nakamura, M. Yokota, F. Sato, Reactor dismantling by abrasive water jet cutting system, JSME Int. J. Series B 36 (1993), https://doi.org/10.1299/jsmeb.36.499.
[41] H. Nakamura, T. Narazaki, S. Yanagihara, Cutting technique and system for biological shield, Nucl. Technol. 86 (1989), https://doi.org/10.13182/nt89-a34267.
[42] M. Hashish, Kinetic power density in waterjet cutting, in: Proceedings of the 22nd International Conference on Water Jetting, 2014.
[43] M. Hashish, Pressure effects in abrasive-waterjet (AWJ) machining, J. Eng. Mater. Technol. 111 (1989) 221–228, https://doi.org/10.1115/1.3226458.
[44] E. Copertaro, F. Perotti, P. Castellini, P. Chiariotti, M. Martarelli, M. Annoni, Focusing tube operational vibration as a means for monitoring the abrasive waterjet cutting capability, J. Manuf. Process. 59 (2020) 1–10, https://doi.org/10.1016/J.JMAPRO.2020.09.040.
[45] E. Copertaro, F. Perotti, M. Annoni, Operational vibration of a waterjet focuser as means for monitoring its wear progression, (n.d.). https://doi.org/10.1007/s00170-021-07534-0/Published.
[46] E. Copertaro, M. Annoni, Airborne acoustic emission of an abrasive waterjet cutting system as means for monitoring the jet cutting capability, Int. J. Adv. Manuf. Technol. 123 (2022) 2655–2667, https://doi.org/10.1007/s00170-022-10317-w.
[47] A.I. Hassan, C. Chen, R. Kovacevic, On-line monitoring of depth of cut in AWJ cutting, Int. J. Mach. Tool Manufact. 44 (2004) 595–605, https://doi.org/10.1016/j.ijmachtools.2003.12.002.
[48] B. Jurisevic, D. Brissaud, M. Junkar, Monitoring of abrasive water jet (AWJ) cutting using sound detection, Int. J. Adv. Manuf. Technol. 24 (2004) 733–737, https://doi.org/10.1007/s00170-003-1752-5.
[49] V. Peržel, P. Hreha, S. Hloch, H. Tozan, J. Valíček, Vibration emission as a potential source of information for abrasive waterjet quality process control, Int. J. Adv. Manuf. Technol. 61 (2012) 285–294, https://doi.org/10.1007/s00170-011-3715-6.
[50] P. Hreha, A. Radvanská, S. Hloch, V. Peržel, G. Królczyk, K. Monková, Determination of vibration frequency depending on abrasive mass flow rate during abrasive water jet cutting, Int. J. Adv. Manuf. Technol. 77 (2015) 763–774, https://doi.org/10.1007/s00170-014-6497-9.
[51] I.A. Popan, V. Bocanet, N. Balc, A.I. Popan, Investigation on feed rate influence on surface quality in abrasive water jet cutting of composite materials, monitoring acoustic emissions, in: S. Hloch, D. Klichová, G.M. Krolczyk, S. Chattopadhyaya, L. Ruppenthalová (Eds.), Advances in Manufacturing Engineering and Materials, Springer International Publishing, Cham, 2019, pp. 105–113.
[52] P. Sutowski, M. Sutowska, W. Kapłonek, The use of high-frequency acoustic emission analysis for in-process assessment of the surface quality of aluminium alloy 5251 in abrasive waterjet machining, Proc. Inst. Mech. Eng. B J. Eng. Manuf. 232 (2017) 2547–2565, https://doi.org/10.1177/0954405417703428.
[53] H. Li, Monitoring the abrasive waterjet drilling of Inconel 718 and steel: a comparative study, Int. J. Adv. Manuf. Technol. 107 (2020) 3401–3414, https://doi.org/10.1007/s00170-020-05246-5.
[54] M.M. Ohadi, A.I. Ansari, M. Hashish, Thermal energy distributions in the workpiece during cutting with an abrasive waterjet, J. Eng. Indust. 114 (1992) 67–73, https://doi.org/10.1115/1.2899760.
[55] M.M. Ohadi, K.L. Cheng, Modeling of temperature distributions in the workpiece during abrasive waterjet machining, J. Heat Tran. 115 (1993) 446–452, https://doi.org/10.1115/1.2910697.
[56] R. Kovacevic, R. Mohan, H.E. Beardsley, Monitoring of thermal energy distribution in abrasive waterjet cutting using infrared thermography, J. Manuf. Sci. Eng. 118 (1996) 555–563, https://doi.org/10.1115/1.2831067.
[57] V. Perzel, M. Flimel, J. Krolczyk, A.S. Sedmak, A. Ruggiero, D. Kozak, A. Stoić, G. Krolczyk, S. Hloch, Measurement of thermal emission during cutting of materials using abrasive water jet, Therm. Sci. 21 (2017) 2197–2203.
[58] N. Yuvaraj, M.P. Kumar, Cutting of aluminium alloy with abrasive water jet and cryogenic assisted abrasive water jet: a comparative study of the surface integrity approach, Wear 362–363 (2016) 18–32, https://doi.org/10.1016/j.wear.2016.05.008.
[59] G. Parma, F.M. Rossi, E. Mossini, M. Giola, E. Macerata, E. Padovani, A. Cammi, M. Mariani, MCNP model of L-54 M nuclear research reactor: development and preliminary verification, J. Radioanal. Nucl. Chem. 318 (2018), https://doi.org/10.1007/s10967-018-6301-7.
[60] G.E.P. Box, W.H. Hunter, S. Hunter, Others, Statistics for Experimenters, John Wiley and sons, New York, 1978.
[61] D.C. Montgomery, Design and Analysis of Experiments, John wiley & sons, 2017.
[62] K.M. Roscioli-Johnson, C.A. Zarzana, G.S. Groenewold, B.J. Mincher, A. Wilden, H. Schmidt, G. Modolo, B. Santiago-Schübel, A Study of the γ-Radiolysis of N,N-Didodecyl-N′,N′-Dioctyldiglycolamide Using UHPLC-ESI-MS Analysis, Solvent Extraction and Ion Exchange, 2016, https://doi.org/10.1080/07366299.2016.1212540.
[63] Predisposal Management of Radioactive Waste, INTERNATIONAL ATOMIC ENERGY AGENCY, Vienna, 2009. https://www.iaea.org/publications/8004/predisposal-management-of-radioactive-waste.
[64] Decommissioning of Nuclear Power Plants, Research Reactors and Other Nuclear Fuel Cycle Facilities, INTERNATIONAL ATOMIC ENERGY AGENCY, Vienna, 2018. https://www.iaea.org/publications/12210/decommissioning-of-nuclear-power-plants-research-reactors-and-other-nuclear-fuel-cycle-facilities.
[65] B.T. Kelly, The behavior of graphite under neutron irradiation, J. Vac. Sci. Technol. 4 (1986) 1171–1178, https://doi.org/10.1116/1.573432.
[66] G. Aydin, Performance of recycling abrasives in rock cutting by abrasive water jet, J. Cent. South Univ. 22 (2015) 1055–1061, https://doi.org/10.1007/s11771-015-2616-5.
[67] A.M.A. Budiea, W.Z. Sek, S.N. Mokhatar, K. Muthusamy, A.R.M. Yusoff, Structural performance assessment of high strength concrete containing spent Garnet under three point bending test, IOP Conf. Ser. Mater. Sci. Eng. 1144 (2021), 012018, https://doi.org/10.1088/1757-899X/1144/1/012018.
[68] M. Hashish, M. Halter, M. McDonald, Abrasive-waterjet Deep Kerfing in Concrete for Nuclear Facility Decommissioning, SPONSORED BY UNITED STATES BUREAU OF MINES UNIVERSITY OF PITTSBURGH WATER JET TECHNOLOGY ASSOCIATION, 1985, p. 97.